Photophysical Properties, Self-Assembly Behavior, and Energy Transfer of Porphyrin-Based Functional Nanoparticles

ARTICLE *in* THE JOURNAL OF PHYSICAL CHEMISTRY C · MAY 2012

Impact Factor: 4.77 · DOI: 10.1021/jp302462j

THE JOURNAL OF PHYSICAL CHEMISTRY C

ARTICLE

pubs.acs.org/JPCC

Porphyrin-Based Functional Nanoparticles: Conformational and Photophysical Properties of Bis-Porphyrin and Bis-Porphyrin Encapsulated Polymer Nanoparticles

Sadananda Mandal,[†] Santanu Bhattacharyya,[†] Victor Borovkov,[*,‡] and Amitava Patra[*,†]

[†]Department of Materials Science, Indian Association for the Cultivation of Science, Kolkata, 700 032, India

[‡]Department of Applied Chemistry, Osaka University, 2-1 Yamada-oka, Suita, Osaka 565-0871, Japan

Supporting Information

ABSTRACT: We first demonstrate the porphyrin-based functional nanoparticles with *syn*-to-*anti* conformational switching from bis-(zinc octaethylporphyrin) [$(ZnOEP)_2$] nanoparticles (NP) to $(ZnOEP)_2$ encapsulated into the semiconducting poly(9-vinylcarbazole) (PVK) polymer NP. The molecular arrangement of $(ZnOEP)_2$ during the formation of nanoparticles has been discussed based on atomic force microscopy (AFM) and other spectroscopic methods. It reveals that the porphyrin nanoparticles are formed by the interbisporphyrin $\pi-\pi$ stacking that is resemble to a single $(ZnOEP)_2$ molecule stabilized by the $\pi-\pi$ interaction between the porphyrin moieties. Furthermore, an efficient excited energy transfer (96%) from the PVK host to the $(ZnOEP)_2$ energy acceptor has been demonstrated that opens further prospects in designing new porphyrin-based functional nanoparticles for the application in effective light harvesting system.

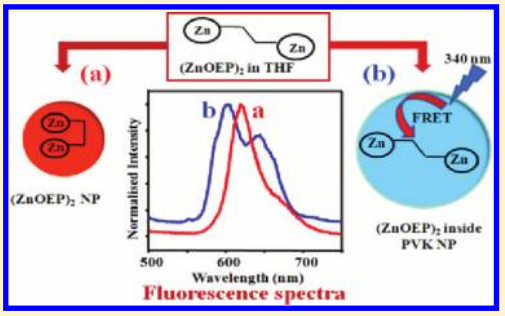

INTRODUCTION

Considerable attention has been paid on porphyrins, metalloporphyrins, and corresponding porphyrinoid-based nanoparticles owing to their potential applications in supramolecular chemistry, light harvesting, photosensitization, photonics, and various sensor technologies.[1−8] Drain et al.[9] reported one of the first syntheses of porphyrin nanoparticles and then demonstrated their enhanced catalytic properties. Also, Nazeeruddin et al.[10] used Zn and Cu complexes of porphyrins in nanocrystalline dye-sensitized solar cells to convert light energy into electrical energy. Meanwhile, Yao et al.[11] reported the narrow size distribution of meso-tetrakis (1-methylpyridinium-4-yl) porphine nanoparticles without self-aggregation. All of the preceding examples clearly demonstrate that porphyrinoids and various porphyrin-based systems are one of the best-suited and versatile chromophoric structures for different light-driven processes. Essentially, the conformational variations of porphyrinoids offer a simple and the effective tool for modulating a wide range of chemical, physicochemical, and spectral properties, hence enhancing their applicability.

In this respect, among a great variety of metalloporphyrins, bis-(zinc octaethylporphyrin), $(ZnOEP)_2$ is particularly attractive owing to its conformational variability (Scheme 1).[12−14] It is well-known that $(ZnOEP)_2$ may exist in *syn* and *anti* forms in organic nonpolar solvents and these conformations can be finely tuned by external ligands or coordinating solvents.[12,14] The *syn* form is due to strong intramolecular hydrophobic and $\pi-\pi$ interactions between the porphyrin macrocycles, while the *syn*-to-*anti* conformational switching is governed by destruction of these intramolecular interactions upon external ligation. There is a considerable difference in the corresponding spectroscopic properties of *syn* and *anti* forms of $(ZnOEP)_2$. For example, in UV−vis absorption spectra, the porphyrin B (Soret) absorption band (S_0-S_2 electronic transition) of *syn* conformation of $(ZnOEP)_2$ is at 397 nm in dichloromethane (DCM) solvent, while in the case of the *anti* form, the B band is bathochromically shifted by 23−30 nm (depending upon the type of external ligand) and often split ($\Delta\lambda$ = 10−12 nm) into two major transitions. The Q bands (S_0-S_1 electronic transition) of both *anti* and *syn* $(ZnOEP)_2$ in DCM appear in the range 560−600 nm, and their relative intensities are varied with changing the conformation.[12,15]

The detailed mechanism of *syn*−*anti* conformational switching in the $(ZnOEP)_2$ molecules and the corresponding spectral modulations have been well-studied to date as in organic solvents[12−15] and in the solid state.[16] Investigations on the porphyrin-based functional nanoparticles are of prime interest from the supramolecular chemistry and nanoscience view points. Another interesting challenge is to design such porphyrin-based nanoparticles with conjugated polymer with a special functionality for future photonic and biophotonic applications. Furthermore, incorporation of a second energy/electron-donating/withdrawing component into nanoparticles (NP) may further enhance the spectral functionality of these nanosystems. In connection with this concept, poly(9-vinylcarbazole) (PVK) is being used as an energy-transfer mediated host due to its specific spectral features well-suited for a porphyrin chromophore.[17] Besides, recently, conjugated polymer NP have attracted considerable interest because of their multifunctional

Received: September 13, 2011
Revised: October 21, 2011
Published: October 30, 2011

Scheme 1. Molecular Structures of PVK (a) and $(ZnOEP)_2$ (b) and Schematic Representations of *syn* (c) and *anti* Forms (d) of $(ZnOEP)_2$

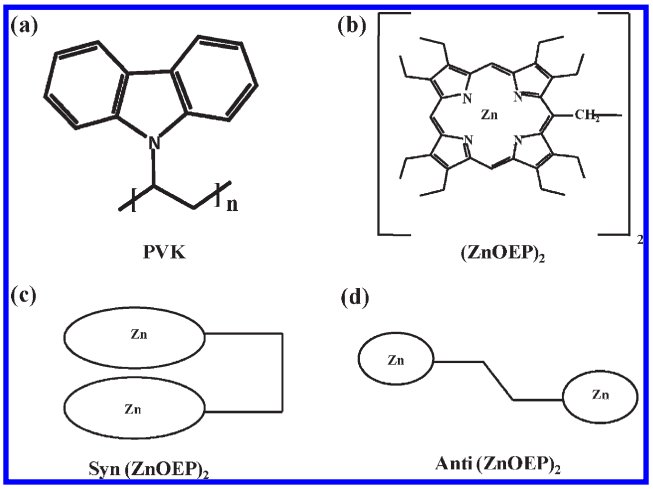

activities in medical imaging, biosensing, drug delivery, photonics, and biophotonics owing to their tunable optical properties, facile synthesis, minor toxicity, and enhanced biocompatibility.[18−20] For example, McNeill and co-workers demonstrated the use of conjugated polymer nanoparticles in the energy-transfer-mediated phosphorescence from metalloporphyrin (Pt(II) octaethylporphyrin)-doped polyfluorene NP and its application to biological oxygen sensing.[21]

However, application of porphyrin-based functional nanoparticles using nanoscopic environment is still in the embryonic stage; therefore, investigations in this field are necessary for in-depth understanding for future prospects in photonic and biophotonic applications. To the best of our knowledge, there is no report on *syn*-to-*anti* conformational switching for $(ZnOEP)_2$ nanoparticles (NP) and the encapsulation of $(ZnOEP)_2$ inside the semiconducting PVK polymer NP formation, respectively. In this paper, we first demonstrate the conformational changes of $(ZnOEP)_2$ during the formation of nanoparticles and $(ZnOEP)_2$ encapsulation inside the semiconducting hole transporting PVK polymer nanoparticles due to change of the environments by using steady state and time-resolved spectroscopy. The molecular arrangement of $(ZnOEP)_2$ during the formation of nanoparticles will be addressed based on atomic force microscopy (AFM) study. Furthermore, an efficient excited energy transfer from PVK host to $(ZnOEP)_2$ energy acceptor is demonstrated that opens further prospects in designing new optical based materials for the application in efficient light harvesting system.

MATERIALS AND METHODS

Poly(9-vinylcarbazole (PVK) (Aldrich), distilled tetrahydrofuran (THF) (MERCK), deionized water (MERCK), and dichloromethane (DCM) (MERCK) were used as received. Bis(zinc octaethylporphyrin) was synthesized according to the previously reported method.[22] Scheme 1 shows the molecular structures of $(ZnOEP)_2$ and PVK.

EXPERIMENTAL PROCEDURES AND INSTRUMENTATIONS

$(ZnOEP)_2$ NP were prepared by the standard reprecipitation method.[23,24] $(ZnOEP)_2$ was dissolved properly in dried THF to maintain the 0.018 mg/mL concentration of $(ZnOEP)_2$. A 500 μL aliquot of this THF solution was rapidly injected into 10 mL of double distilled water under vigorous stirring for 10−15 min. Then, the obtained solution was ultrasonicated for 15 min. As a result, an aqueous solution of $(ZnOEP)_2$ NP was obtained. Then, to avoid aging of the porphyrin NP, THF was removed from aqueous solution by partial vacuum evaporation for 1 h followed by filtration through a 0.2 μm filter paper. Finally, a stable aqueous solution of $(ZnOEP)_2$ NP was obtained. Pure PVK NP were synthesized following our previously reported reprecipitation method.[25]

The $(ZnOEP)_2$ inside PVK NP system was prepared by similar reprecipitation method.[26] In this particular case, THF solutions of $(ZnOEP)_2$ and PVK were mixed thoroughly to maintain the 0.018 mg/mL concentration of $(ZnOEP)_2$ and 1 mg/mL concentration of PVK, followed by ultrasonication for 20 min to obtain a clear mixed solution. Then, a 500 μL aliquot of the THF solution was rapidly injected into double distilled water under vigorous stirring for 10−15 min. Then, similar ultrasonication, vacuum evaporation, and filtration through 0.2 μm filter as in the case of preparation of $(ZnOEP)_2$ NP were subsequently carried out. Finally, $(ZnOEP)_2$ encapsulated PVK NP was obtained.

The morphological characters and sizes of $(ZnOEP)_2$ NP, pure PVK NP and $(ZnOEP)_2$ encapsulated PVK NP were done by field emission scanning electron microscopy (FE-SEM, JEOL, JSM-6700F) and atomic force microscopy (AFM, VEECO, dicp-II). Room temperature optical absorption spectra were taken by a UV−vis spectrophotometer (SHIMADZU). Room temperature photoluminescence spectra were recorded by a Fluoromax-P (HORIBA JOBIN YVON) photoluminescence spectrophotometer. The steady-state anisotropy measurement was performed by an L-format dual-polarizer setup (FL-1044) attached with a Fluoromax-P (HORIBA JOBIN YVON) photoluminescence spectrophotometer. The steady-state anisotropy (r) is calculated using eq 1.[27]

$$r = \frac{I_{VV} - GI_{VH}}{I_{VV} + 2GI_{VH}} \quad (1)$$

$$G = \frac{I_{HV}}{I_{HH}} \quad (2)$$

Here, I_{VV} is the intensity with vertical excitation and vertical emission, I_{VH} is the intensity with vertical excitation and horizontal emission, and G is defined as the ratio of the intensity with horizontal excitation and vertical emission to the intensity with horizontal excitation and horizontal emission. For the time correlated single photon counting (TCSPC) measurements, the samples were excited at 405 nm using a picosecond diode laser (IBH Nanoled-07) in an IBH Fluorocube apparatus. The typical full width at half-maximum (fwhm) of the system response using a liquid scatter was about 90 ps. The repetition rate was 1 MHz. The fluorescence decays were collected at a Hamamatsu MCP photomultiplier (C487802). The fluorescence decays were analyzed using IBH DAS6 software. For 340 nm excitation, a NANO-LED IBH 340 was used. The following equation[28] was used to analyze the experimental time-resolved fluorescence decays, $P(t)$:

$$P(t) = b + \sum_i^n \alpha_i \exp\left(-\frac{t}{\tau_i}\right) \quad (3)$$

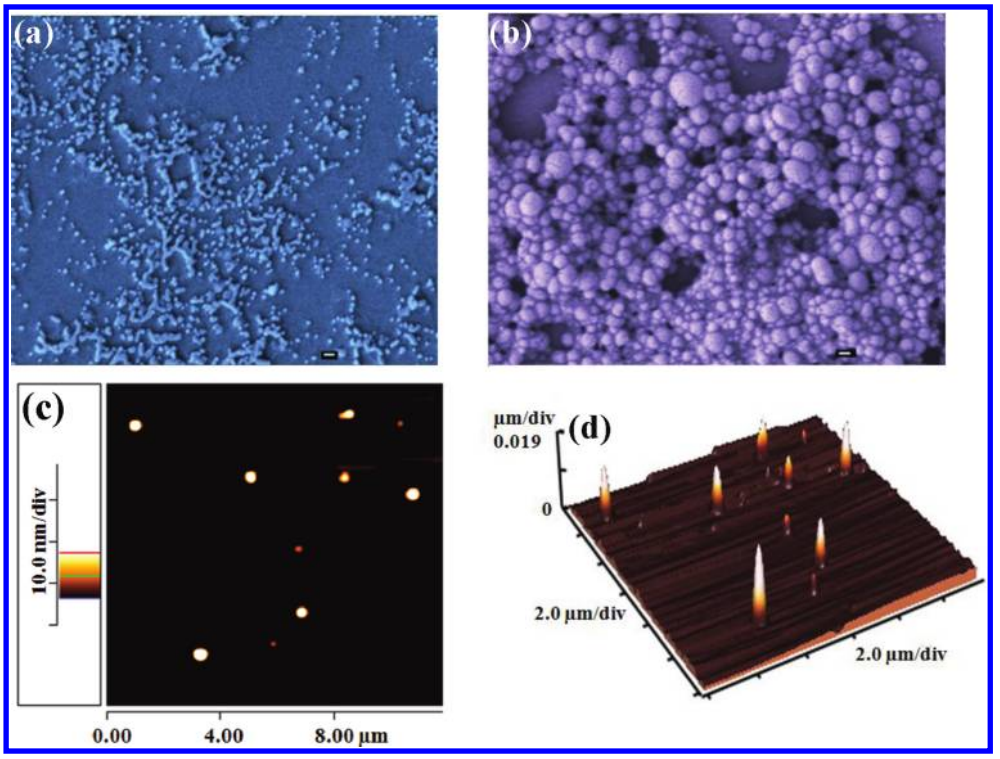

Figure 1. FE-SEM images of $(ZnOEP)_2$ nanoparticles (a) (Scale bar = 100 nm), $(ZnOEP)_2$ inside PVK NP (b) (Scale bar =100 nm). AFM image of $(ZnOEP)_2$ nanoparticles 2D (c) and 3D (d).

Here, n is the number of discrete emissive species, b is a baseline correction ("dc" offset), and α_i and τ_i are the pre-exponential factors and excited-state fluorescence lifetimes associated with the i^{th} component, respectively.[28] For multiexponential decays, the average lifetime,$\langle\tau\rangle$, was calculated from the following equation:[28]

$$\langle\tau\rangle = \sum_{i=1}^{n} \alpha_i \tau_i^2 / \sum_{i=1}^{n} \alpha_i \tau_i \qquad (4)$$

RESULTS AND DISCUSSION

Structural and Conformational Study. Figure 1 shows the FE-SEM images of $(ZnOEP)_2$ NP (a) and $(ZnOEP)_2$ inside PVK NP (b). These images unambiguously confirm the formation of spherical porphyrin nanoparticles and PVK nanoparticles by the reprecipitation method used in this study. The average sizes are found to be 50 nm, 150 and 150 nm for $(ZnOEP)_2$ NP, pure PVK and $(ZnOEP)_2$ encapsulated PVK NP, respectively. As evident from the SEM images the size of $(ZnOEP)_2$ NP is comparatively smaller than that of pure PVK NP (see Supporting Information, Figure S1) and $(ZnOEP)_2$ encapsulated PVK NP. The size of pure polymer nanoparticles remains essentially unchanged after the encapsulation of $(ZnOEP)_2$ molecules. McNeill and co-workers also reported that the particle size and morphology are not affected by the presence of dye molecules in the case of conjugated polymer nanoparticles doped with a small amount of fluorescent compound.[29] In the case of the $(ZnOEP)_2$ encapsulated PVK NP system, the concentration of $(ZnOEP)_2$ in the stock THF solution is much lower than that of PVK, thus resulting in PVK to serve as a size-determinant component of the whole system. During the injection of THF solution of $(ZnOEP)_2$ into water under the stirring condition, THF molecules quickly diffuse into bulk water, and $(ZnOEP)_2$ molecules are exposed to the aqueous environment. Since water is a poor solvent for hydrophobic $(ZnOEP)_2$, the molecules tend to aggregate to avoid contact with water, thus yielding nanoparticles. AFM images of $(ZnOEP)_2$ NP also unambiguously confirm the formation of nanoparticles (Figure 1(c) and (d)). In our present study, the measured diameter and height of the particles are 60−80 and 20 nm, respectively, using AFM. The nanoparticle diameter measured with SEM is 50 nm. The diameter measured with AFM is larger compared to SEM due to tip convolution and may be a result of exaggeration during the measurement in the tapping mode that is often observed in the case of soft materials.[30] Recently, Gesquiere et al.[30] measured the size of MEH-PPV/PCBM nanoparticles using TEM, AFM, and the measured diameter is 28 nm by TEM and the measured diameter and height of the particles are 63 and 12 nm, respectively, using AFM.

The growth mechanism of porphyrin nanoparticles has been also rationalized by analyzing the AFM data. According to the crystallographic data, the intra and inter Zn−Zn distances (The intra Zn−Zn distance is the distance between two Zn ions of the same $(ZnOEP)_2$ molecule, and the inter Zn−Zn distance is the distance between two Zn ions of adjacent $(ZnOEP)_2$ molecules in the crystal lattice) of the *syn* form of $(ZnOEP)_2$ are calculated to be 0.48 and 0.59 nm, respectively.[31] As seen from the high resolution of the AFM image (Figure 2), the distance between two steps of the neighboring molecular layers is about 0.60 nm and matches well with the inter Zn−Zn distance. This implies that the formation of porphyrin nanoparticles is governed by the interporphyrin $\pi-\pi$ stacking. This is similar to the driving forces organizing a single $(ZnOEP)_2$ molecule because the *syn* conformation is also due to the strong hydrophobic and $\pi-\pi$ interactions between two porphyrin moieties. Thus, this clearly

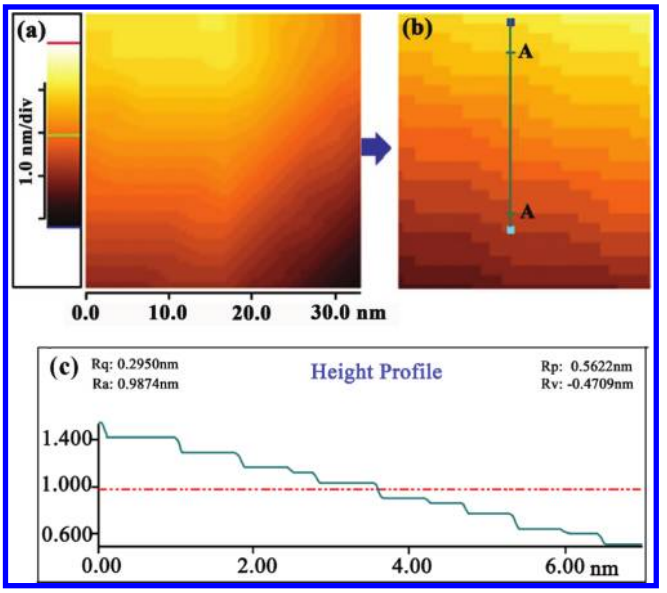

Figure 2. AFM images of $(ZnOEP)_2$ NP in high resolution (a) and (b); and (c) height profile of (b).

indicates that there is no change in the *syn* conformation of $(ZnOEP)_2$ during the formation of nanoparticles, which is additionally supported by spectroscopic measurements.

Steady-State and Time-Resolved Spectroscopy Study. Figure 3A shows the UV−vis spectra of $(ZnOEP)_2$ in various environments. In general, metalloporphyrins feature two well-defined absorption regions, the so-called high-energy B band (also known as Soret band) and low-energy Q bands. The Soret absorption band corresponds to S_0-S_2 electronic transitions, while the Q bands correspond to S_0-S_1 electronic transitions.[32] Both the B and Q bands arise from $\pi-\pi^*$ electronic transitions. The UV−vis spectrum of $(ZnOEP)_2$ in DCM has been reported previously[15] and shows blue-shifted and a highly intense Soret band at 397 nm and two relatively weak Q bands at 556 and 594 nm, respectively, which are the inherent characteristics of a *syn* conformational $(ZnOEP)_2$ molecule. The UV−vis spectral feature of $(ZnOEP)_2$ nanoparticles exhibits essentially the same spectral pattern as that of a $(ZnOEP)_2$ molecule in DCM. The band positions of the Soret band at 400 nm and Q bands of $(ZnOEP)_2$ NP are almost similar with a $(ZnOEP)_2$ molecule in DCM. A small difference in the spectral shape of $(ZnOEP)_2$ NP and $(ZnOEP)_2$ in DCM is observed. In particular, the calculated fwhm are 43 and 34 nm for $(ZnOEP)_2$ NP and $(ZnOEP)_2$ in DCM, respectively. Some broadening of the $(ZnOEP)_2$ NP spectrum is due to the solid-state interbisporphyrin aggregation through $\pi-\pi$ interactions, which is consistent with the previous results reported for the porphyrin-containing systems in a KBr matrix, as for $(ZnOEP)_2$[16] and for monomeric zinc octaethylporphyrin.[33] The same positions of Soret and Q bands imply that the intramolecular conformations of $(ZnOEP)_2$ both in the NP form and in the DCM solution are essentially invariable hence being *syn*. In contrast, the Soret absorption band of the $(ZnOEP)_2$ in the PVK NP system is totally different from the two above-discussed systems. The Soret absorption band maximum is bathochromically shifted up to 420 nm for $(ZnOEP)_2$ encapsulated in PVK NP, while the second B transition is seen as a shoulder at 437 nm. This spectral profile is similar to that of *anti* form of $(ZnOEP)_2$ induced by weakly interacting ligands, such as

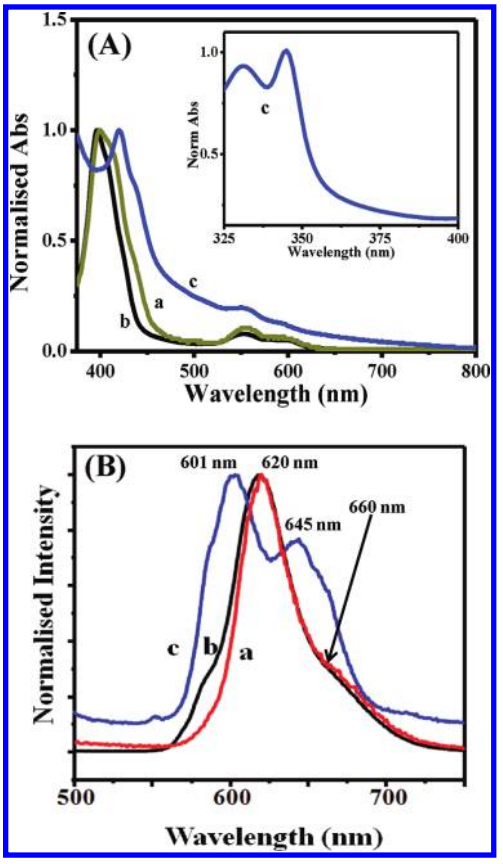

Figure 3. (A) UV−vis and (B) fluorescence spectra of $(ZnOEP)_2$ (a) nanoparticles form, (b) in DCM solution, and (c) inside PVK nanoparticles.

alcohols, upon lowering the temperature.[12,34] Therefore, it is reasonable to conclude that the PVK matrix may also act as a weakly interacting ligand for $(ZnOEP)_2$ inside the PVK NP. The high-energy transition at 345 nm is assigned for the PVK component absorption (inset Figure 3A), as also can be seen in the PVK NP system alone (see Supporting Information, Figure S2A). Thus, the UV−vis spectral data clearly reveals that $(ZnOEP)_2$ is in the *syn* conformation in the nanoparticle form and in the *anti* conformation inside PVK NP.

Figure 3B shows the fluorescence spectra of $(ZnOEP)_2$ in the same environment as the corresponding UV−vis spectra. The fluorescence spectral feature of a $(ZnOEP)_2$ molecule in DCM solution and in the form of nanoparticles is also essentially the same. Both systems possess two emission bands, Q^*_{X00} and Q^*_{X01}, with maxima at 620 and 660 nm (as a shoulder), respectively. This spectral pattern has been already reported for the corresponding *syn* conformation of $(ZnOEP)_2$ in DCM[13] and in chloroform,[22] indicating the *syn* conformation of $(ZnOEP)_2$ in the nanoparticle form. On the other hand, the destruction of the intramolecular $\pi-\pi$ interactions between two porphyrin moieties yields the corresponding *anti* conformation of $(ZnOEP)_2$ in the case of $(ZnOEP)_2$ inside the PVK nanoparticle. A significant change in the fluorescence spectrum with two well-defined emission band with the maxima at 601 and 645 nm is observed, which is in a good agreement with the emission exhibited by the *anti* conformation of related zinc-containing bis-porphyrin molecules[22,35] and $(ZnOEP)_2$ itself in the presence of external ligands (see the Discussion below). Therefore, these results along

with the above-discussed absorption data unambiguously indicate that $(ZnOEP)_2$ exists in the *anti* conformation inside the PVK nanoparticles.

Now, a question arises, what is the driving force of this conformational switching with changing the environments? The initial conformation of $(ZnOEP)_2$ in the THF solution is *anti* because THF acts as an efficient external ligand[36] for zinc porphyrins thus inducing the corresponding *anti* form in $(ZnOEP)_2$ as well-documented by the corresponding spectral patterns being specific for this type of conformation (see Supporting Information, Figure S3A and S3B).[12,14,15] During the injection of the THF solution into water (poor solvent for hydrophobic $(ZnOEP)_2$) and subsequent evaporation of THF, the $(ZnOEP)_2$ molecules become ligand free, while bulk water is not able to form a coordination complex with hydrophobic $(ZnOEP)_2$ due to its insolubility. This forces a switch of their conformation from *anti* to *syn*, while the *syn* conformation of $(ZnOEP)_2$ itself is stabilized in the nanoparticles by the strong intermolecular $\pi-\pi$ interactions between the two zinc porphyrin macrocycles as in the case of noncoordinative solvents and the solid state.[12−16,22,35] However, the $(ZnOEP)_2$ molecules inside the PVK NP are in the *anti* conformation due to the following possible reasons: (i) $(ZnOEP)_2$ molecules are not able to switch their conformation from *anti* back to *syn* due to the excessive rigidity of the PVK NP, and (ii) there may be an attraction interaction between a tertiary nitrogen atom of the carbazole moiety of the PVK and Zn ion of the porphyrin because PVK acts as a weak ligand, like an alcohol, the binding of which may be considerably enhanced in the solid state conditions. To find out the most plausible reason, we have carried out the following experiment. At first, $(ZnOEP)_2$ encapsulated in PVK NPs are prepared by the miniemulsion method (Supporting Information and Figure S4). After encapsulation in PVK NP (prepared by miniemulsion method), the $(ZnOEP)_2$ molecule remains in the *syn* conformation, as in the case of DCM solvent. This was supported by the corresponding spectral data. In this case, the Soret band appears at 400 nm (hump) that is almost at the same position as found for $(ZnOEP)_2$ in DCM (at 397 nm), and both systems possess the major emission band at 620 nm. (Supporting Information, Figures S4 and S5). However, the $(ZnOEP)_2$ molecule is in the *anti* conformation after the encapsulation by PVK NP (prepared by reprecipitation method), since initially THF is used as a solvent. These two observations strongly imply that the conformation (*syn*/*anti*) of the $(ZnOEP)_2$ molecule encapsulated in PVK NP is due to the restricted motion of the molecule inside the polymer matrix. Second, we have studied the absorption and fluorescence properties of $(ZnOEP)_2$ in DCM solvent in the absence and in the presence of PVK (weight ratio of $(ZnOEP)_2$ and PVK is 9.0×10^{-3}) to evaluate the attractive interaction between a tertiary nitrogen atom of the carbazole moiety of PVK and a Zn atom of the porphyrin. It shows that the absorption and the emission band positions are intact after the addition of PVK (Supporting Information, Figure S5). This observation also suggests that there is no substantial interaction between the tertiary nitrogen atom of the carbazole moiety of PVK and Zn atom of porphyrin in the concentration range 0−1 mg/mL of PVK that corresponds to the spectral measurements. Thus, this analysis suggests that the conformation (*syn*/*anti*) of the $(ZnOEP)_2$ molecule encapsulated in PVK NP is essentially governed by the rigidity of the polymer matrix, although some weak binding interactions may also play an additional role to stabilize the *anti* conformation in the solid state environment.

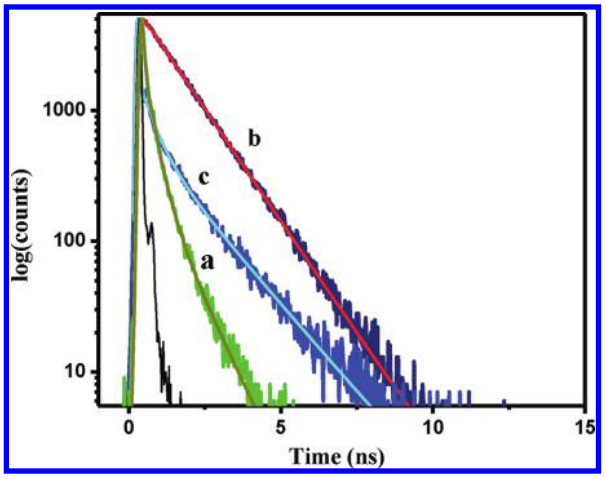

Figure 4. Decay curves of $(ZnOEP)_2$ (a) in nanoparticles form, (b) in DCM solution, and (c) inside PVK nanoparticles (Excitation wavelength at 405 nm).

The steady-state anisotropy value increases from 0.02 to 0.16 for $(ZnOEP)_2$ in DCM, and $(ZnOEP)_2$ inside PVK NP, respectively, which further confirmed the restricted motion of the molecule inside the polymer matrix.

In order to gain further insight in the excited-state relaxation pathways of these systems, the fluorescence decay curves of $(ZnOEP)_2$ in DCM, $(ZnOEP)_2$ NP and $(ZnOEP)_2$ in PVK NP have been measured (Figure 4). The decay curve of $(ZnOEP)_2$ in DCM is reasonably well-fitted by a monoexponential decay (χ^2 = 1.25) with a lifetime of 1.24 ns (Table 1), which is consistent with the previously obtained results.[13] The decay curves of $(ZnOEP)_2$ NP in water and $(ZnOEP)_2$ inside PVK NP are fitted by triexponential decay curves (the χ^2 values are 0.84 and 1.08 for $(ZnOEP)_2$ NP in water and $(ZnOEP)_2$ inside PVK NP, respectively). The fitting components of the $(ZnOEP)_2$ NP systems are 0.06 ns (82%), 0.28 ns (15%), and 0.85 ns (3%) with the average decay time of 0.11 ns. In the case of $(ZnOEP)_2$ inside PVK NP, the corresponding components are 0.06 ns (39%), 0.65 ns (26%), and 1.90 ns (35%), and the average decay time is 0.68 ns. The decay curve of *anti* conformation of $(ZnOEP)_2$ in THF is fitted by a monoexponential decay (χ^2 = 0.98). The decay time is 1.69 ns (Supporting Information, Figure S3C). We have also calculated the radiative and nonradiative decay rates of different systems to evaluate their influence on decay time. The observed emission lifetime (τ_{obs}) is combined with the fluorescence quantum yield (ϕ^0) to determine the radiative and nonradiative rate separately for all the systems. The following equations[27] are used to determine these rates:

$$k_r = \frac{\varphi^0}{\tau} \tag{5}$$

$$k_{nr} = \frac{(1-\varphi^0)}{\tau} \tag{6}$$

Where k_r and k_{nr} are the radiative and nonradiative rates constant, respectively, ϕ^0 is the quantum yield of the molecule, and τ is the average decay time. As seen from Table 1, the nonradiative decay rates are 7.9×10^8, 9×10^9, and 14.5×10^8 s^{-1} for $(ZnOEP)_2$ in DCM, $(ZnOEP)_2$ NP, and in PVK NP, respectively. The nonradiative decay rate is highest in $(ZnOEP)_2$ NP. As discussed above, in water (poor solvent), hydrophobic $(ZnOEP)_2$ molecules

Table 1. Fluorescence Decay Parameters, Radiative, and Nonradiative Decay Rates of $(ZnOEP)_2$ in Various Systems[a]

system	λ_{em} (nm)	τ_1(ns) (a_1)	τ_2(ns) (a_2)	τ_3 (ns) (a_3)	<τ> (ns)	QY $(ZnOEP)_2$	$\kappa_r \times 10^{-7}$ (s^{-1})	$\kappa_{nr} \times 10^{-8}$($s^{-1}$)
$(ZnOEP)_2$ NP in water	620	0.28 (0.15)	0.06 (0.82)	0.85 (0.03)	0.11	0.010	0.11	90.0
$(ZnOEP)_2$ inside PVK NP	601	0.65 (0.26)	1.90 (0.35)	0.06 (0.39)	0.68	0.014	2.00	14.5
$(ZnOEP)_2$ in DCM	620	1.24 (1)	–	–	1.24	0.024	1.9	7.9

[a] Excitation wavelength at 405 nm.

tend to aggregate to form nanoparticles, and hence, intermolecular interaction as well as $\pi-\pi$ stacking is increased, which enhances the nonradiative rate due to close proximity of the neighboring porphyrin molecules. It is interesting to note that radiative decay rate increases from 0.11×10^7 to 2.00×10^7 s^{-1} for $(ZnOEP)_2$ NP and $(ZnOEP)_2$ encapsulated PVK NP, respectively, due to enhancement of hydrophobicity and refractive index in the polymer matrix.[37,38]

Energy Transfer Study. It is clearly seen that there is a good overlap between the absorption spectrum of $(ZnOEP)_2$ and emission spectrum of PVK (Supporting Information, Figure S2B), indicating the possibility of an energy transfer from the energy donor PVK host to the acceptor $(ZnOEP)_2$ guest molecule. In general, fluorescence resonance energy transfer (FRET) is a process involving the radiationless (nonradiative) transfer of energy from a "donor" fluorophore to an appropriate "acceptor" fluorophore. This process arises from the dipole–dipole interactions and strongly depends on the center-to-center distance of donor and acceptor. According to the Förster theory,[39] the rate of the energy transfer for an isolated single donor–acceptor pair separated by a distance r is given by the following:

$$k_T(r) = \frac{1}{\tau_D}\left(\frac{R_0}{r}\right)^6 \quad (7)$$

where τ_D is the lifetime of the donor in the absence of the acceptor, R_0 is known as the Förster distance, the distance at which the transfer rate $k_T(r)$ is equal to the decay rate of donor in the absence of acceptor. The Förster distance (R_0) is defined as the following:

$$R_0^6 = \frac{9000(In10)\kappa^2\varphi_D}{128\pi^5 Nn^4}J(\lambda) \quad (8)$$

where ϕ_D is the quantum yield of donor in the absence of acceptor, N is Avogadro's number, n is the refractive index of medium, $J(\lambda)$ is the spectral overlap integral that is defined as the following:

$$J(\lambda) = \int_0^\infty F_D(\lambda)\varepsilon_A(\lambda)\lambda^4 d\lambda \quad (9)$$

where $F_D(\lambda)$ is the normalized emission spectrum of donor, $\varepsilon_A(\lambda)$ is the absorption coefficient of acceptor at wavelength λ (in nm), and κ^2 is the orientation factor of two interacting dipoles. The value of κ^2 depends on the relative orientation of donor and acceptor dipoles. For randomly oriented dipoles $\kappa^2 = {}^2/_3$, and it varies between 0 and 4 for the cases of orthogonal and parallel dipoles, respectively. For our donor–acceptor system, the calculated overlap integral is found to be 1.42×10^{14} $M^{-1}cm^{-1}nm^4$, and the calculated Förster distance is 23.3 Å.

Figure 5(A) shows the fluorescence spectra of pure PVK NP (a) and $(ZnOEP)_2$ encapsulated PVK NP (b–d) with varying the concentration of $(ZnOEP)_2$ after excitation at 340 nm. An enhancement of the quenching efficiency of PVK is observed

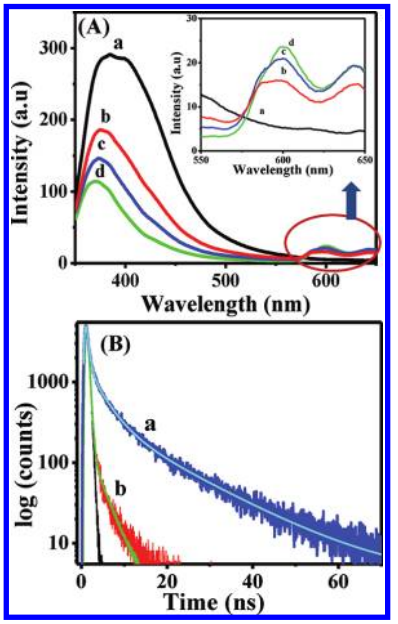

Figure 5. (A) Fluorescence spectra of PVK NP (excitation = 340 nm) (a) pure PVK NP and (b–d) ratios of $(ZnOEP)_2$/ PVK increases. (B) Decay curves of PVK NP (a) pure PVK NP and (b) $(ZnOEP)_2$ inside PVK NP (excitation wavelength at 340 nm).

with increasing the concentration of $(ZnOEP)_2$. The fluorescence intensity quenching are found to be 43%, 58%, and 69% for the concentrations of $(ZnOEP)_2$ equal to 0.18, 0.36, and 1.8 wt %, respectively. To rationalize the energy transfer mechanism using the FRET method, we measured the fluorescence decay time of PVK with and without $(ZnOEP)_2$. Figure 5(B) shows the decay curves of pure PVK NP and with $(ZnOEP)_2$ encapsulated PVK NP (for 1.8 wt % $(ZnOEP)_2$) at the excitation wavelength of 340 nm that corresponds to the absorption band of PVK. The decay curve of pure PVK NP is fitted by triexponential decay (χ^2 = 1.09). The corresponding components of pure PVK NP are 3.59 ns (15%), 14.92 ns (4%), and 0.59 ns (81%) with the average decay time of 1.61 ns (Table 2). The decay curve of $(ZnOEP)_2$ encapsulated PVK NP is fitted by biexponential decay (χ^2 = 1.26). The components are 0.05 ns (99%) and 3.20 ns (1%), and the average decay time is extremely short, 0.08 ns (Table 2). The decrease of decay time of PVK in the presence of $(ZnOEP)_2$ molecules confirms the host–guest energy transfer from PVK to $(ZnOEP)_2$. The energy transfer efficiency can be calculated by using the following equation:[27]

$$\varphi_{ET} = 1 - \frac{\tau_{DA}}{\tau_D} \quad (10)$$

Where τ_{DA} and τ_D are the average decay times of $(ZnOEP)_2$ encapsulated PVK NP and pure PVK NP, respectively. The calculated energy transfer efficiency is 96%, and the rate of energy

Table 2. Fluorescence Decay Parameters of Pure PVK NP and $(ZnOEP)_2$ inside PVK NP[a]

system	λ_{em} (nm)	τ_1(ns) (a_1)	τ_2(ns) (a_2)	τ_3(ns) (a_3)	<τ> (ns)
PVK NP	390	3.59 (0.15)	14.92 (0.04)	0.59 (0.81)	1.61
$(ZnOEP)_2$ inside PVK NP	372	0.05 (0.99)	3.20 (0.01)	–	0.08

[a] Excitation wavelength at 340 nm.

transfer is 13.78 × 10^9 s^{-1} as obtained by using eq 7. This high efficiency of energy transfer compared to photoluminescence quenching is not only due to the dipole−dipole interaction between the donor and acceptor but also excitonic energy diffusion[26] throughout the polymer chain may increase the energy transfer phenomena. However, further investigations in this field are necessary for in-depth understanding this phenomenon.

CONCLUSION

In this report, we have synthesized bis(zinc octaethylporphyrin), $(ZnOEP)_2$ nanoparticles, and $(ZnOEP)_2$ encapsulated into semiconducting poly(9-vinylcarbazole) (PVK) polymer nanoparticles in water for the first time. Steady-state study and AFM analysis suggest that the conformations of bis-porphyrin nanoparticles and bis-porphyrin inside PVK NP are *syn* and *anti*, respectively. The molecular arrangement of $(ZnOEP)_2$ during the formation of nanoparticles has been addressed based on AFM and various spectroscopic studies. A strong photoluminescence quenching and the shortening of fluorescence decay time of host PVK confirm the efficient energy transfer (96%) from PVK to bis-porphyrin with the rate of energy transfer is 13.78 × 10^9 s^{-1}. An efficient excited energy transfer from PVK host to $(ZnOEP)_2$ energy acceptor opens further prospects to design new porphyrin-based functional nanoparticles for the application in efficient light harvesting system.

ASSOCIATED CONTENT

Supporting Information. Synthetic procedure of $(ZnOEP)_2$ encapsulated in PVK nanoparticles by miniemulsion method; Figure S1 showing the FE-SEM image of Pure PVK NP; Figure S2 showing (A) UV−vis spectrum of pure PVK NP and (B) overlap spectra between the absorption spectrum of $(ZnOEP)_2$ and the emission spectrum of pure PVK NP; Figure S3 showing $(ZnOEP)_2$ in THF solvent, (A) absorption spectrum, (B) fluorescence spectrum, and (C) fluorescence decay time spectrum; Figure S4 showing (A) absorption spectra and (B) fluorescence spectra, (a) $(ZnOEP)_2$ in DCM and (b) $(ZnOEP)_2$ encapsulated in PVK NP; and Figure S5 showing (A) absorption spectra and (B) flourescence spectra of (a) $(ZnOEP)_2$ in DCM (b) mixture of $(ZnOEP)_2$ and PVK in DCM. This material is available free of charge via the Internet at http://pubs.acs.org.

AUTHOR INFORMATION

Corresponding Author

*(A.P.) E-mail: msap@iacs.res.in; Phone: (91)-33-2473-4971; Fax: (91)-33-2473-280. (V.B.) E-mail: victrb@chem.eng.osaka-u.ac.jp; Phone: (81)-6-6879-4128; Fax: (81)-6-6879-7923.

ACKNOWLEDGMENT

The CSIR is gratefully acknowledged for financial support. S.M. and S.B. thank CSIR for awarding fellowship.

REFERENCES

(1) Khlebtsov, B.; Panfilova, E.; Khanadeev, V.; Bibikova, O.; Terentyuk, G.; Ivanov, A.; Rumyantseva, V.; Shilov, I.; Ryabova, A.; Loshchenov, V.; Khlebtsov, N. G. *ACS Nano* **2011**, *5*, 7077–7089.
(2) Chen, S.-G.; Yu, Y.; Zhao, X.; Ma, Y.; Jiang, X.-K.; Li, Z.-T. *J. Am. Chem. Soc.* **2011**, *133*, 11124–11127.
(3) Fercher, A.; Borisov, S. M.; Zhdanov, A. V.; Klimant, I.; Papkovsky, D. B. *ACS Nano* **2011**, *5*, 5499–5508.
(4) Villari, V.; Mazzaglia, A.; Trapani, M.; Castriciano, M. A.; de Luca, G.; Romeo, A.; Scolaro, L. M.; Micali, N. *J. Phys. Chem. C* **2011**, *115*, 5435–5439.
(5) Drain, C. M.; Smeureanu, G.; Patel, S.; Gong, X.; Garno, J.; Arijeloye, J. *New J. Chem.* **2006**, *30*, 1834–1843.
(6) Ji, H. X.; Hu, J. S.; Wan, L. J. *Chem. Commun.* **2008**, 2653–2655.
(7) Hasobe, T.; Imahori, H.; Kamat, P. V.; Ahn, T. K.; Kim, S. K.; Kim, D.; Fujimoto, A.; Hirakawa, T.; Fukuzumi, S. *J. Am. Chem. Soc.* **2005**, *127*, 1216–1228.
(8) Ishida, Y.; Shimada, T.; Masui, D.; Tachibana, H.; Inoue, H.; Takagi, S. *J. Am. Chem. Soc.* **2011**, *133*, 14280–14286.
(9) Gong, X.; Milic, T.; Xu, C.; Batteas, J. D.; Drain, C. M. *J. Am. Chem. Soc.* **2002**, *124*, 14290–14291.
(10) Nazeeruddin, Md. K.; Humphry-Baker, R.; Officer, D. L.; Campbell, W. M.; Burrell, A. K.; Grätzel, M. *Langmuir* **2004**, *20*, 6514–6517.
(11) Ou, Z.; Yao, H.; Kimura, K. *J. Photochem. Photobiol. A: Chem.* **2007**, *189*, 7–14.
(12) Borovkov, V. V.; Lintuluoto, J. M.; Inoue, Y. *J. Phys. Chem. B* **1999**, *103*, 5151–5156.
(13) Borovkov, V. V.; Lintuluoto, J. M.; Sugiura, M.; Inoue, Y.; Kuroda, R. *J. Am. Chem. Soc.* **2002**, *124*, 11282–11283.
(14) Borovkov, V. V.; Lintuluoto, J. M.; Hembury, G. A.; Sugiura, M.; Arakawa, R.; Inoue, Y. *J. Org. Chem.* **2003**, *68*, 7176–7192.
(15) Borovkov, V. V.; Lintuluoto, J. M.; Inoue, Y. *J. Am. Chem. Soc.* **2001**, *123*, 2979–2989.
(16) Borovkov, V. V.; Harada, T.; Inoue, Y.; Kuroda, R. *Angew. Chem., Int. Ed.* **2002**, *41*, 1378–1381.
(17) Morgado, J.; Cacialli, F.; Iqbal, R.; Moratti, S. C.; Holmes, A. B.; Yahioglu, G.; Milgromand, L. R.; Friend, R. H. *J. Mater. Chem.* **2001**, *11*, 278–283.
(18) Wu, C.; Szymanski, C.; Cain, Z.; McNeill, M. *J. Am. Chem. Soc.* **2007**, *129*, 12904–12905.
(19) Wu, C.; Bull, B.; Szymanski, C.; Christensen, K.; McNeill, M. *ACS Nano* **2008**, *2*, 2415–2423.
(20) Rahim, N. A. A.; McDaniel, W.; Bardon, K.; Srinivasan, S.; Vickerman, V.; So, P. T. C.; Moon, J. H. *Adv. Mater.* **2009**, *21*, 3492–3496.
(21) Wu, C.; Bull, B.; Christensen, K.; McNeill, J. *Angew. Chem., Int. Ed.* **2009**, *48*, 2741–2745.
(22) Borovkov, V. V.; Lintuluoto, J. M.; Inoue, Y. *Helv. Chim. Acta* **1999**, *82*, 919–934.
(23) Kashani-Motlagh, M. M.; Rahimi, R.; Kachousangi, M. J. *Molecules* **2010**, *15*, 280–287.
(24) Perepogu, A. K.; Bangal, P. R. *J. Chem. Sci.* **2008**, *120*, 485–491.
(25) Bhattacharyya, S.; Sen, T.; Patra, A. *J. Phys. Chem. C* **2010**, *114*, 11787–11795.
(26) Wu, C.; Zheng, Y.; Szymanski, C.; McNeill, J. *J. Phys. Chem. C* **2008**, *112*, 1772–1781.
(27) Lakowicz, J. R. *Principles of Fluorescence Spectroscopy*, 3rd ed.; Kluwer Academic/Plenum Publishers: New York, 1999; pp 354−464.

(28) Patra, A.; Baker, G. A.; Baker, S. N. *J. Lumin.* **2005**, *111*, 105–111.
(29) Wu, C.; Peng, H.; Jiang, Y.; McNeill, J. *J. Phys. Chem. B* **2006**, *110*, 14148–14154.
(30) Tenery, D.; Worden, J. G.; Hu, Z.; Gesquiere, A. J. *J. Lumin.* **2009**, *129*, 423–429.
(31) Fujii, I.; Borovkov, V. V.; Inoue, Y. *Anal. Sci.* **2006**, *22*, x77–x78.
(32) *Porphyrins and Metalloporphyrins*; Smith, K. M., Ed.; Elsevier: Amsterdam, The Netherlands, 1975.
(33) Borovkov, V. V.; Harada, T.; Hembury, G. A.; Inoue, Y.; Kuroda, R. *Angew. Chem.* **2003**, *115*, 1788–1791.
(34) Borovkov, V. V.; Lintuluoto, J. M.; Fujiki, M.; Inoue, Y. *J. Am. Chem. Soc.* **2000**, *122*, 4403–4407.
(35) Valli, L.; Casilli, S.; Giotta, L.; Pignataro, B.; Conoci, S.; Borovkov, V. V.; Inoue, Y.; Sortino, S. *J. Phys. Chem. B* **2006**, *110*, 4691–4698.
(36) Schauer, C. K.; Anderson, O. P.; Eaton, S. S.; Eaton, G. *Inorg. Chem.* **1985**, *24*, 4082–4086.
(37) Larson, D. R.; Ow, H.; Vishwasrao, H. D.; Heikal, A. A.; Wiesner, U.; Webb, W. W. *Chem. Mater.* **2008**, *20*, 2677–2684.
(38) Toptygin, D.; Savtchenko, R. S.; Meadow, N. D.; Roseman, S.; Brand, L. *J. Phys. Chem. B* **2002**, *106*, 3724–3734.
(39) Förster, T. *Discuss. Faraday Soc.* **1959**, *27*, 7–17.